



In vitro drug release behavior of Ce-doped nano-bioactive glass carriers under oxidative stress

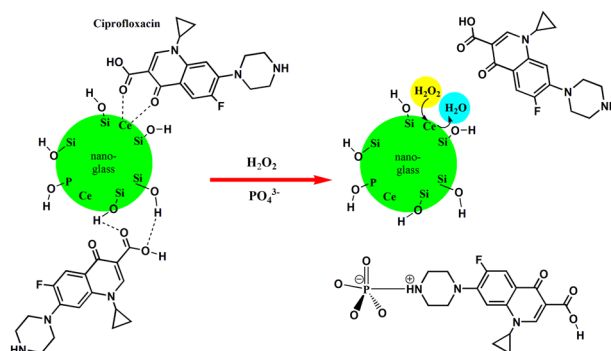
Mohammad M. Farag¹ · Zainab M. Al-Rashidy² · Manar M. Ahmed¹

Received: 29 June 2018 / Accepted: 10 January 2019 / Published online: 22 January 2019
© Springer Science+Business Media, LLC, part of Springer Nature 2019

Abstract

Ce-containing bioactive glasses are known to decrease reactive oxygen activities inside the body. That is because of their excellent catalytic activities which come from the fast interchange of Ce^{3+}/Ce^{4+} oxidation states. This research was mainly aimed at preparing new Ce-doped nano-bioactive glasses based on $60SiO_2-(10-x)B_2O_3-25CaO-5P_2O_5-xCeO_2$, in mole% ($x = 0$ and 5 mol%) as multifunctional bone fillings. Moreover, the glasses were used as a delivery system for ciprofloxacin to intensely solve the bone infection complications. Nevertheless, there were no previous works studied of the nature immersing solution effect on the drug release behavior from Ce-doped nano-bioactive glass carriers. Therefore, phosphate-free and phosphate-containing buffer solutions with/without superoxide species (H_2O_2) were used to investigate the efficacy of this drug delivery system in different environment. The results showed that Ce addition enhanced the formation of apatite layer and cell viability. Moreover, the percentage of released drug was apparently affected by the glass composition and nature of soaking fluid, specifically, in the media containing superoxide species (H_2O_2). In conclusion, the prepared Ce-doped glass nanoparticles illustrated multifunctional bone filling material, but when it intended to be utilized as a drug delivery system, the nature of surrounding medium have to be taken into consideration.

Graphical Abstract



1 Introduction

Improving the properties and efficiency of bone grafting materials, generally, and bioactive glasses, specifically, by adding therapeutic ions (e.g. Fe, Ag, Cu, and Mg), have become important targets in the bone diseases treatment. Addition of such ions to the bioactive glasses yielded multifunctional glass materials. Cerium is one such therapeutic ions. Cerium is a rare earth element; it has drawn the attention as potential therapeutic dopant in the biomaterials. Cerium oxide nanoparticles (nanoceria) are one of cerium

✉ Mohammad M. Farag
mmfaragnrc@gmail.com

¹ Glass Research Department, National Research Centre, 33 El- Behooth Str., Dokki, Cairo 12622, Egypt

² Refractories, Ceramics and Building Materials Department, National Research Centre, 33 El-Behooth Str., Dokki, Cairo 12622, Egypt

compounds used widely in different biomedical applications. They have shown a protective cell agent against the damage resulted from the reactive oxygen species (ROS) which produced from normal oxygen metabolism [1]. That is because of their ability to switch between Ce^{4+} and Ce^{3+} oxidation states [2]. ROS are byproducts of normal oxygen metabolism that can cause oxidative damage to macromolecules in biological cells. Two dominant ROS, superoxide (O_2^-) and hydrogen peroxide (H_2O_2), are neutralized in cells by specific enzymes, primarily superoxide dismutase (SOD) and catalase, respectively. Oxidative stress is the intracellular imbalance between ROS and the enzymes that are involved in their detoxification. It has been involved in several diseases and disorders, including Parkinson's and Alzheimer's disease, cardiovascular disease and even tumor development [3]. Therefore, there have been several researches incorporated cerium in different bioactive glasses to be used as antioxidant bioactive materials [4–13]. However, inclusion of Ce in glasses has altered their capability to form hydroxyapatite layer in the body fluid. That is because of an affinity of Ce ions to interact with phosphate ions to form insoluble $CePO_4$ crystals, and thus decrease a possibility of apatite formation [12, 14]. This made a limitation to increase addition of Ce percentages in glass compositions. Nevertheless, Ce addition showed a significant effect to decrease the bioactivity of glasses prepared by melting method, but its effect can be diminished for sol-gel glasses which was characterized by enormous surface area and reactivity [7]. Therefore, synthesis of Ce-doped glasses combines between high bioactivity and potential catalase mimetic activity is possible by using sol-gel method.

Moreover, bioactive glasses acquire outstanding biocompatibility when boron is included in the glass structure. Boron is known to affect a variety of metabolic actions, whereas it interacts with calcium, vitamin D, and magnesium, which are important in bone metabolism [15]. It accumulates in bone in concentrations that depend on the amount of its consumption [16]. Its deficiency in animals leads to growth, weakness of bone, and abnormal bone development [15]. It was found that dietary boron can be stimulated by bone regeneration of the midpalatal suture in response to expansion [17]. Also, boron showed remarkable antibacterial activity against bacteria, yeast, and fungi [18, 19]. Thus, boron has been included into different types of bioactive glasses prepared either by melting or sol-gel route. Where, it enhanced the bioactivity and biocompatibility by improving hydroxyapatite formation, stimulating angiogenesis, and enhancing proliferation and expression of osteogenesis-related genes in osteoblasts [20–23].

Bioactive glasses nanoparticles are a good candidate to be used as a drug-delivery system due to their extraordinary surface area and biocompatibility. Appropriately, bioactive

glass carriers have been modified by doping with specific ions to tailor and make drug release more controllable [24–28]. However, most of previous studies on Ce-doped glasses only addressed the effect of Ce on the glass structure, dissolution, antibacterial, bioactivity, biocompatibility, and/or biocatalytic properties [4–13], and there were few works concerned with using such glasses as drug carriers [25]. Even the studies dealing with use of Ce-doped glass as drug carriers did not focus mainly on the influence of soaking fluid nature on the drug release profile. Although some studies showed that the oxidative activity and bioactivity of Ce-containing glasses were affected by the nature of surrounding solutions. For instance, it was found that presence of phosphate in the immersion fluids decreased the catalase mimetic activity of ceria nanoparticles and Ce-containing glasses [12, 29, 30].

Since using of cerium-containing bioactive glasses as a novel bioactive and drug carriers to treat different bone diseases, there is an urgent need to study the behavior of the drug release in the presence of ROS and phosphates species in the soaking medium, and thus simulating the drug release in a phosphate-rich and oxidative stress environment. In this study, we synthesized Ce-doped bioactive glass nanoparticles to deliver Ce ions which are known as excellent antioxidant ions. As well as, the behavior of antibacterial drug release from Ce-containing nanobioactive glass carrier in the presence of ROS was reported. Such carrier was designed as bone regenerative, antioxidant, and antibacterial bone filling.

2 Materials and methods

2.1 Glass preparation

Different glass compositions were prepared based on $60SiO_2-(10-x)B_2O_3-25CaO-5P_2O_5-xCe_2O$, in mole% ($x = 0$ and 5 mole%). The glass compositions are represented in Table 1. The following chemicals with analytical grade used as received to synthesize glasses by a quick alkali-mediated sol-gel method [31]. TEOS (tetraethyl ortho silicate), boron alkoxide, $Ca(NO_3)_2 \cdot 4H_2O$, TEP (triethyl phosphate) and $Ce(NH_4)_2(NO_3)_6$ (ammonium cerium (IV) nitrate, ethanol (EtOH), nitric acid (HNO_3), and ammonia. In a typical synthesis of nano bioactive glass (NBG), TEOS was added to a mixture of 2 M HNO_3 and ethanol solution. TEOS:

Table 1 Compositions of the investigated glasses in mole %

Code	SiO_2	B_2O_3	CaO	P_2O_5	CeO_2
C0	60	10	25	5	–
C5	60	5	25	5	5

EtOH: H₂O was 1: 8: 10 molar ratio. After complete hydrolysis of TEOS, TEP, Ca(NO₃)₂·4H₂O and ammonium cerium (IV) nitrate added to the solution, respectively, with 30 min time interval, and the solution left to stir for 4 h. Concentrated ammonia solution was dropped into the solution while vigorously stirring. The sol was rapidly transformed to white gel which stirred mechanically to avoid the formation of bulk gel. Thereafter, the obtained gel was dried at 50 °C in the oven for 2 days to remove the residual water and ethanol. Finally, the dry gel powder was calcined and heated with a rate of 5 °C/min at 600 °C in air for 30 min.

2.2 Characterizations

The dry gels were characterized by differential scanning calorimetry analysis and thermogravimetric analysis (DSC-TGA) using a Pyris Diamond TG/DTA thermal analyzer using an airflow of 200 ml min⁻¹ and heating from 35 to 1000 °C at 10 °C min⁻¹, in order to determine the temperatures of getting rid of organic components and nitrates in the gel, as well as, to determine the glass transition temperature (T_g) and the crystallization temperature (T_c). X-ray diffraction (XRD) was carried out using a Philips PW1390 X-ray diffractometer (U.S.D.). The XRD-patterns were recorded at room temperature in the 2θ range from 10 to 70° in 0.02° steps counting for 19 s per step using CuKα radiation (1.5418 Å). Transmission electron microscope (TEM) was used to investigate particle size and morphology. The infrared absorption spectra of bioactive glass powder samples were analyzed at room temperature in the wave number range of 4000–400 cm⁻¹ by Fourier transform infrared (FTIR) using JASCO FT/IR-4600. The prepared samples each of 2 mg were mixed with 200 mg KBr in an agate mortar and pressed into a pellet. For each sample, the FTIR spectrum was normalized with a blank KBr pellet.

2.3 In vitro bioactivity test

The in vitro bioactivity assessment was evaluated in simulated body fluid (SBF) which prepared according to Kokubo and Takadama [32]. The glass samples were shaped in disks by compressing 0.2 g of glass powder uniaxially in stainless steel mold with 8 mm in diameter under pressure of 2 MPa. The disks were immersed in polyethylene bottles contained SBF. The immersed fluid was completely collected and replaced by fresh SBF at predetermined times (1, 2, 4, 8, and 15 days), and the concentrations of the released ions (Ca, P, and Ce ions) from the samples into the solutions were measured by using either inductively coupled plasma atomic emission spectroscopy (ICP-AES) using Agilent5100 Synchronous Vertical Dual View (SVDV) or

colorimetric kits (BIODIGNOSTIC, Egypt), as well as, the change of pH of SBF measured as a function of time. Moreover, the change of samples surfaces before and after immersion in SBF was investigated by a field emission scanning electron microscope coupled with energy dispersive X-ray analysis; Model Quanta 250 FEG (Field Emission Gun) attached with EDX Unit (Energy Dispersive X-ray Analyses), with accelerating voltage 30 KV.

2.4 Biocompatibility test

2.4.1 Cytocompatibility evaluation

A human lung fibroblast normal cell line (WI-38 cells) was propagated in Dulbecco Eagle's medium (DMEM) supplemented with 10% heat-inactivated fetal bovine serum, 1% L-glutamine, HEPES buffer, and 50 µg/ml gentamicin. All cells were maintained at 37 °C in a humidified atmosphere with 5% CO₂ and were subcultured two to three times a week.

The cells were seeded in a 96-well plate at a cell concentration of 1 × 10⁴ cells per well in 100 µl of growth medium. Fresh medium containing different concentrations of the glass powders were added after 24 h of seeding, and the incubation was continued for 48 h. Three wells were used for each concentration of the samples. The numbers of viable cells yield were determined by the MTT test. Briefly, the media were removed from the 96-well plate and replaced with 100 µl of fresh culture RPMI 1640 medium without phenol red, then 10 µl of the 12 mM MTT stock solution (5 mg of MTT in 1 mL of PBS) was added to each well including the untreated controls.

The 96-well plates were then incubated at 37 °C in 5% CO₂ atmosphere for 4 h. Eighty-five microlitre aliquot of the media was removed from the wells, and 50 µl of DMSO was added to each well and mixed thoroughly with the pipette and incubated at 37 °C for 10 min. The optical density was measured at a wavelength of 590 nm with the microplate reader (SunRise, TECAN, Inc, USA) to determine the number of viable cells and the percentage of viability, calculated as:

$$(\text{ODt}/\text{ODc}) \times 100\%$$

Where OD_t is the mean optical density of wells treated with the sample and OD_c is the mean optical density of the untreated cells. The relation between surviving cells and sample concentrations was plotted. Sample analysis results were obtained in triplicate from three separate experiments.

The cytotoxicity concentration (CC₅₀), the concentration required to cause toxic effects in 50% of intact cells was estimated from graphic plots of the dose response curve for each concentration using Graphed Prism software (San Diego, CA,USA) [33].

2.4.2 Morphological observation of cells

After the end of the incubation period, media were aspirated, and then the cells were fixed with formalin. Crystal violet (1%) was used to stain the fixed cells, where it was added to each well for at least 30 min. The cytopathic effect (morphological alterations) was microscopically detected using inverted microscope (CKX41; Olympus, Japan). The cells morphology was examined under light microscope for normal and treated cells under $\times 40$ lens.

2.5 Antibacterial activity

Gram negative bacteria; *Escherichia coli* (ATCC 25922) and *Pseudomonas aeruginosa* (ATCC 27853), and gram positive bacteria; *Bacillus subtilis* (ATCC 6633), and *Staphylococcus aureus* (ATCC 6538) were used for in vitro evaluation of the antimicrobial activity. The inoculum was prepared and the antibacterial activity carried out according the previous literatures [34–38]. Antibacterial activity was performed for C0 and C5 glass powders by seeding 50 ml of bioassay medium (nutrient agar) with 100 μ l of cell suspension (contained 1.5×10^8 CFU/ml) of 24 h old test organisms. Thereafter, 200 mg of the glass powder was placed on the surface of each seeded plate with tested organisms, and then placed in the refrigerator for 1 h followed by incubation at 37 °C for 24 h, and finally, the zones of inhibition were measured in mm.

2.6 In vitro drug release study

Ciprofloxacin was used as a drug model. It is a synthetic broad spectrum fluoroquinolone antibiotic. It is active against a wide variety of aerobic gram-negative and gram-positive bacteria. The drug was loaded into glass nanoparticles by immersing 50 mg glass powder in 10 ml of ciprofloxacin solution (1 mg/ml) for 24 h under stirring. Thereafter, the powder was collected by filtration by filter paper and dried at 60 °C. The amounts of adsorbed drug were determined indirectly by measuring the concentration of non-adsorbed drug in the solutions and their absorbance were measured by UV/VIS spectroscopy (UNICO UV2000) at wavelength 277 nm.

The drug release behavior was studied by immersing 50 mg of glass-loaded drug in 10 ml phosphate-free solution (0.05 M tris-HCl buffer, pH 7.4) and phosphate-contained solution (phosphate buffer saline (PBS), pH 7.4 [39]) to study the effect of phosphate content on the drug release profile. As well as, the release was investigated in 0.05 M tris-HCl and PBS contained 0.5 M of H₂O₂ (pH 7.4) to mimic the drug release in ROS medium. The drug release was evaluated at 37 °C up to 7 days. At each predetermined time (1, 3, 6, 12 h, 1, 2, 3, 5, 7 days), 2 ml of immersed solution was collected

and replaced by 2 ml fresh one. The collected solutions were kept at -20 °C up till the measurement. The concentrations of released drug were determined by measuring the absorbance by UV/VIS spectroscopy at wavelength 277 nm and plotting it on the standard curve.

2.6.1 Drug releasing mechanism

The drug release mechanism was investigated by fitting the drug release profiles to the Higuchi model. This model was used extensively to define the diffusion controlled processes of released drug from the porous carrier [40]. This model is given by the following equation:

$$Q = k.t^{0.5}$$

Where, Q is the percentage of drug released at time t , and k is the release rate constant.

2.7 Statistical analysis

All experimental data stated in this work were expressed as the average \pm standard deviation (SD) for $n = 3$ and were analyzed using standard analysis of Student's t -test. The level of significance (p -value) is set at <0.05 .

3 Results and discussion

3.1 DTA-TGA

The differential thermal analysis (DTA) and thermogravimetric analysis (TGA) of samples C0 and C5 are shown in Fig. 1. The TGA curves showed that both dry gels underwent three mass losses in temperature ranges; 80–300, 300–450, and 450–550 °C for C0, and 20–200, 200–300, and 300–490 °C for C5. The first weight losses corresponded to endothermic peak in DTA at 128 and 90 °C for C0 and C5, respectively, which associated with the removal of physically adsorbed water from the raw material [41]. The second ones attributed to exothermic peak in the DTA curves at 300 and 282 °C, respectively, due to the loss of organics (i.e. alkoxy groups). The third losses represented by endothermic peaks at 512 and 518 °C, respectively, corresponded to the glass transition temperatures and the elimination of residual nitrates introduced as metal nitrate in the preparation of the sol [42]. These results confirmed that all residuals removed before 550 °C for both samples. Therefore, the temperature of 600 °C was chosen for the stabilization of two glasses. The final exothermic peaks located on the DTA curves for C0 and C5 at 743 and 880 °C, respectively, with no corresponding weight loss were likely due to the crystallization temperatures of glass samples.

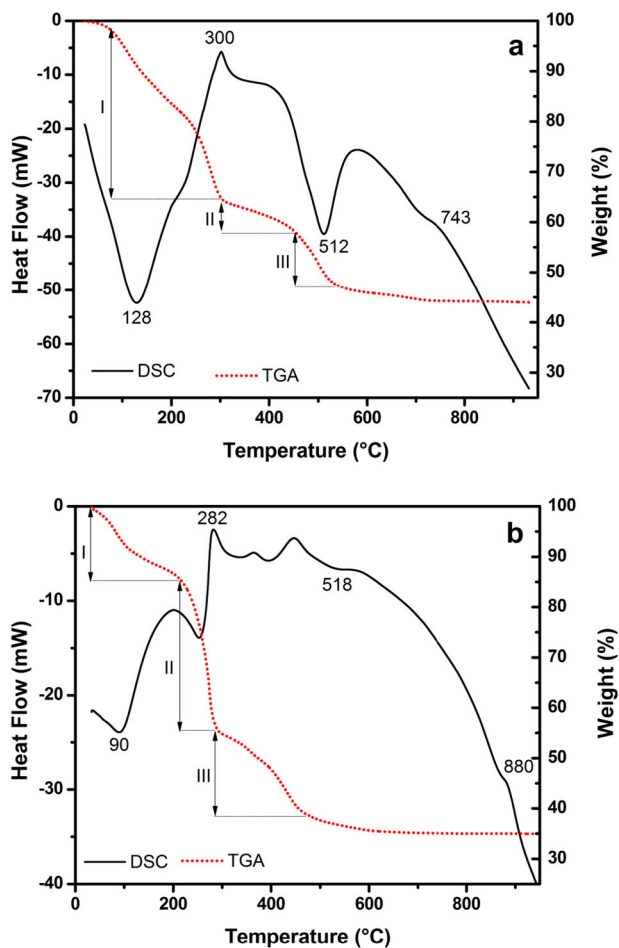


Fig. 1 DSC and TGA of C0 **a** and C5 **b** dry gel samples

3.2 XRD

The glasses were analyzed by XRD technique after calcination step to determine the formation of any crystalline phases as a result of this calcination process. Figure 2 shows the XRD patterns of Ce-free and Ce-doped glasses (C0 and C5, respectively). A broad hump with weak diffraction peak at $2\theta \sim 32$ which was likely attributed to partial crystallization of glass to form calcium silicate, Ca_2SiO_4 (JCPDS # 29-0369) [43] was observed for C0 glass, which attributed to the amorphous structure of the silica framework of the glass. However, weak diffraction peaks were observed at 2θ 28.6, 33.3, 47.0, and 56.4 in case of C5 glass which assigned to formation of CeO_2 crystals, where, these peaks are characteristic peaks of CeO_2 according to JCPDS # 34-0394. This result was confirmed by TEM analysis, as it was showed in the following paragraphs.

3.3 TEM

Glass particle sizes and morphology were examined by TEM analysis. Figure 3a, b presents TEM micrographs of

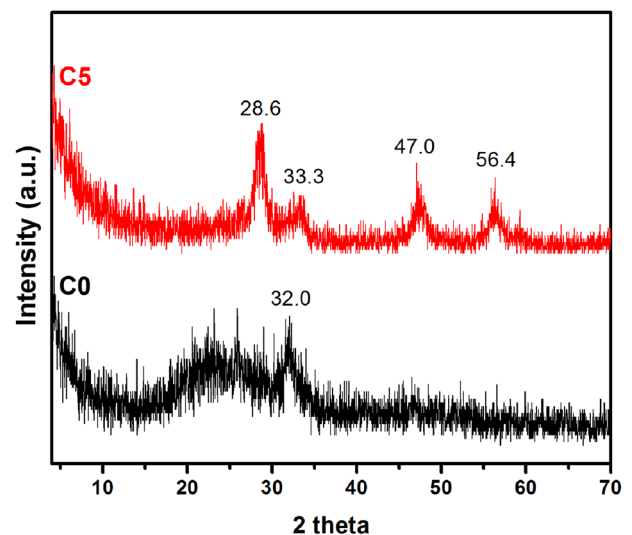


Fig. 2 XRD patterns of C0 and C5 glass samples

C0 and C5, respectively. It can be noted from the figure that both glass powders were exhibited in nano-scale. They ranged from 10 to 20 nm for C0 glass particles with semi-spherical shapes, while, the glass particle sizes were decreased by Ce doping (C5 glass) to be ranged from 6 to 10 nm particles and kept with their semi-spherical shapes. Nevertheless, now diffraction pattern observed from C0 glass, while, it was noticed from C5 glass in some regions of glass particle (Fig. 3c) at almost (111), (200), (220), and (311) crystallographic planes (in accordance with JCPDS # 34-0394). This diffraction pattern was attributed to CeO_2 crystalline spheres of about 5 nm in diameter, as confirmed by XRD analysis. Accordingly, CeO_2 was likely phase-separated and precipitated through the silicate glass network to form minute spheroids in the glass.

3.4 FTIR

Figure 4 illustrates the FTIR spectra of C0 and C5 glasses. Si–O–Si bending vibration modes were observed at 466 cm^{-1} for both undoped (C0) and Ce-doped (C5) glasses [6]. Whereas, the P–O bending mode was detected at 422 cm^{-1} [44]. Doublets at 570 and 600 cm^{-1} were attributed to O–P–O antisymmetric bending of phosphate group in the form of crystalline orthophosphate PO_3^{4-} . The orthophosphate groups in isolated crystalline nano regions weaken connectivity of glass structure and serve as nucleation sites in SBF [6, 45]. Moreover, the band noticed at 800 cm^{-1} was assigned to the O–Si–O bending mode of orthosilicate SiO_4^{4-} [46]. The band allocated at 877 cm^{-1} was corresponded to Si–O–2NBO stretching for Ce-doped glass (C5) but not observed for undoped glass (C0). Accordingly, the addition of Ce_2O_3 to the glass composition acted mainly as a network modifier thus disrupts the silicate network and

Fig. 3 TEM micrographs **a** and **b** for C0 and C5, respectively, and diffraction pattern **c** for C5 glass

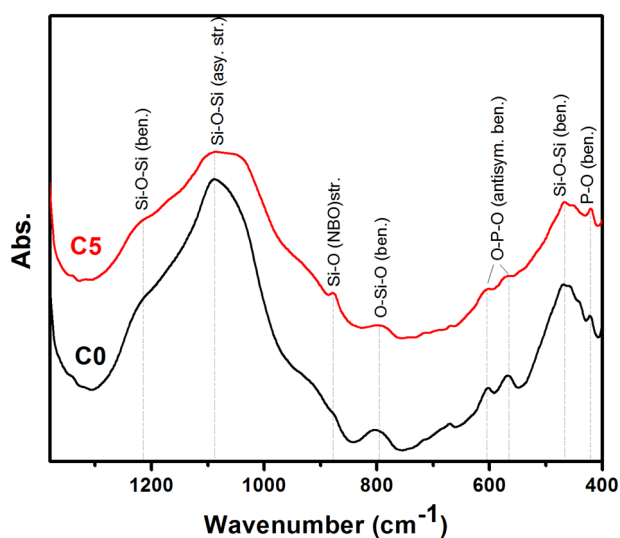
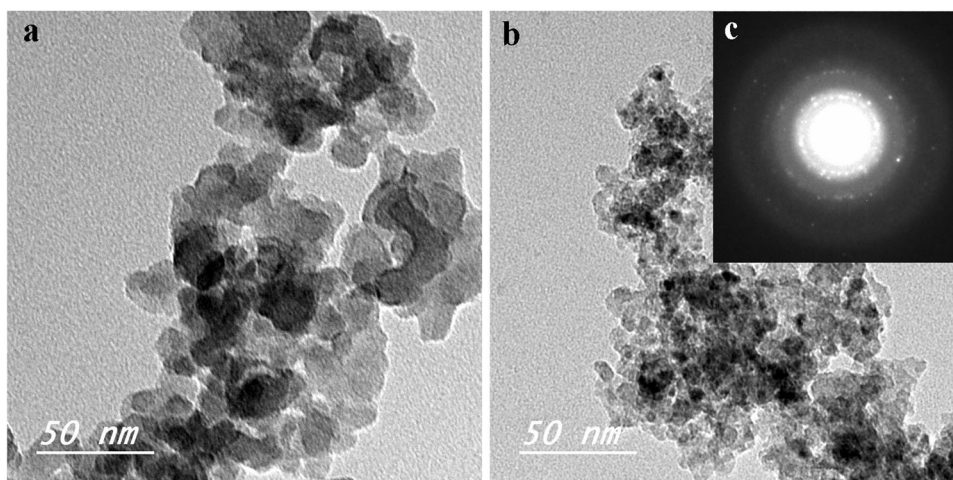


Fig. 4 FTIR spectra of C0 and C5 glass samples

increased the number of non-bridging oxygens (NBOs) [47]. The NBO promotes glass leaching which is considered beneficial in enhancing apatite formation thus increase bioactivity [48]. Si–O–Si asymmetric stretching vibration was noted at 1087 cm^{-1} and 1085 cm^{-1} for C0 and C5 glasses, respectively [6]. The shoulder remarked at about 1220 cm^{-1} was attributed to Si–O–Si bending mode [49].

3.5 In vitro bioactivity and degradation assessment

A widely used method for assessing the capability of a material to bond to living bone tissue is its ability to form a bone-like apatite layer on their surface upon immersion in SBF. This bone-like apatite layer enables the materials to make direct contact with human bone living cells. Figure 5 shows the SEM and EDX analysis of the surface of the C0 and C5 samples before and after immersion in SBF for 15 days. Before SBF immersion SEM shows that their

surfaces were heterogeneous. Their corresponding EDX spectra show a large amount of Si and a small amount of Ca and P for both samples. Signals of Ce atom was also observed for C5 confirming their presence in the glass matrix. After 15 days of SBF immersion SEM showed aggregation of spherical particles on sample surfaces. The corresponding EDX spectrum of the newly formed surface layer showed high concentrations of Ca and P in comparison to Si for both samples. The Ca/P molar ratios were found 1.98 and 1.76 for C0 and C5, respectively. The Ca/P ratio of C5 was closer to the stoichiometric hydroxyapatite ratio (1.67) than C0 sample. However, a modification of the glass with cerium did not alter the in vitro bioactivity of the glass; on the contrary, the bioactivity was enhanced by cerium addition, and this was evident from Ca^{2+} and Si^{4+} ions concentrations in SBF. However, a presence of Ce in melt glass was found to suppress the in vitro bioactivity [12, 14] due to formation of less soluble CePO_4 crystals on the glass surface. In the case of sol-gel glass, it is characterized by much higher surface area and pore numbers than the melt glass, and it shows a high reactivity in the body fluid. In our case, cerium was increased the number of NBOs (as confirmed by FTIR analysis), and so, the reactivity of glass surface was increased in SBF to form the apatite layer. Thus, we able to add higher percentage of cerium (up to 5 mole%) than that added to previously prepared sol-gel glasses [7] without altering the glass bioactivity.

The change of pH of C0 and C5 was investigated by measuring pH values of incubated SBF at predetermined times. Figure 6a shows the variation of SBF as a function of time after immersing in SBF solution up to 15 days. It can be noted from the figure that the changes in the pH values of SBF incubated samples C0 and C5 were approximately similar. The pH values increased during the first day of immersion to 7.64 and 7.58 for C0 and C5, respectively. This was as a result of a rapid ion exchange between Ca^{2+} and H^+ or H_3O^+ in SBF solution which caused an increase

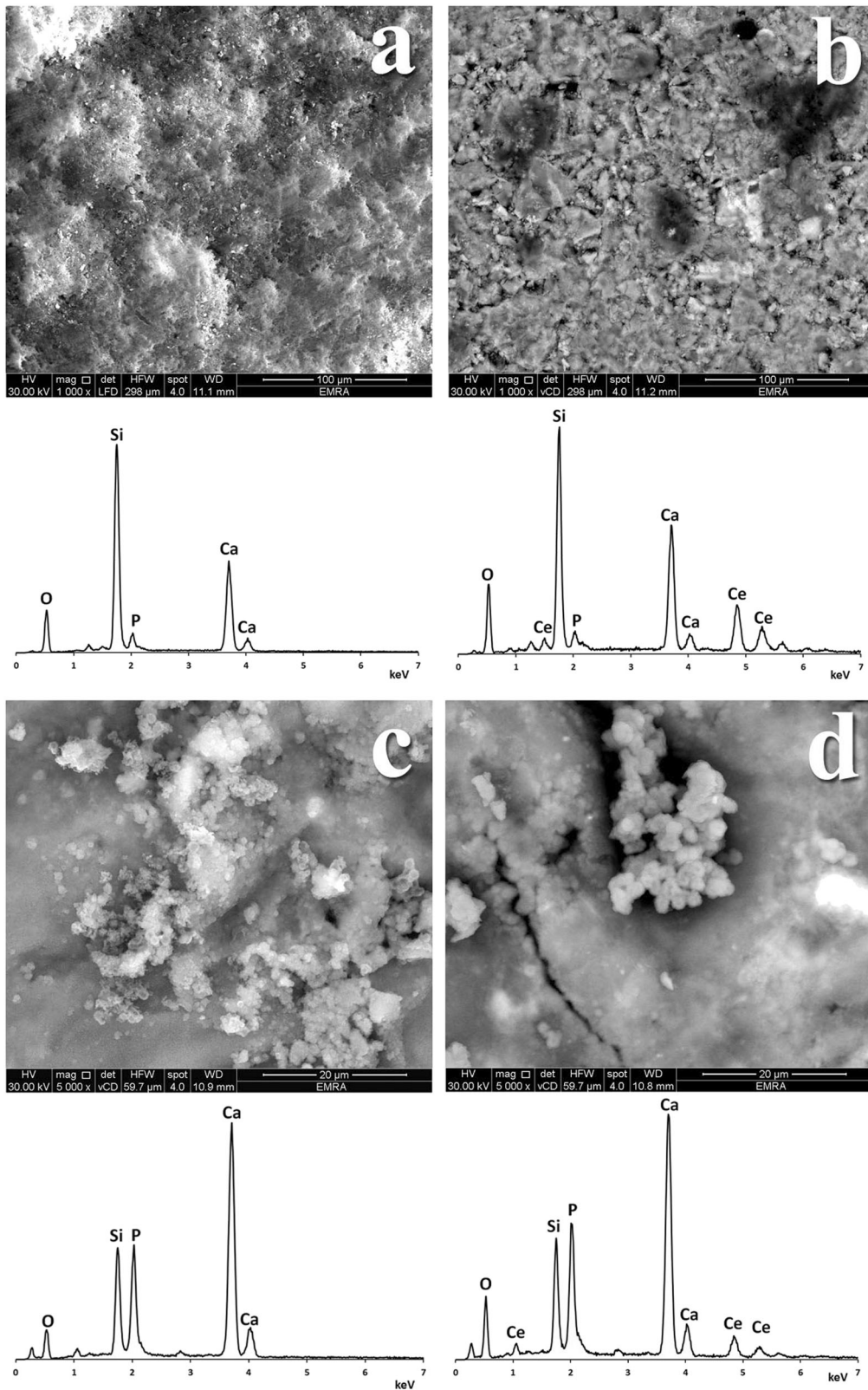


Fig. 5 SEM micrographs accompanied by EDX analysis of the samples C0 and C5 before (a, b, respectively) and after (c, d, respectively) immersion in SBF for 15 days

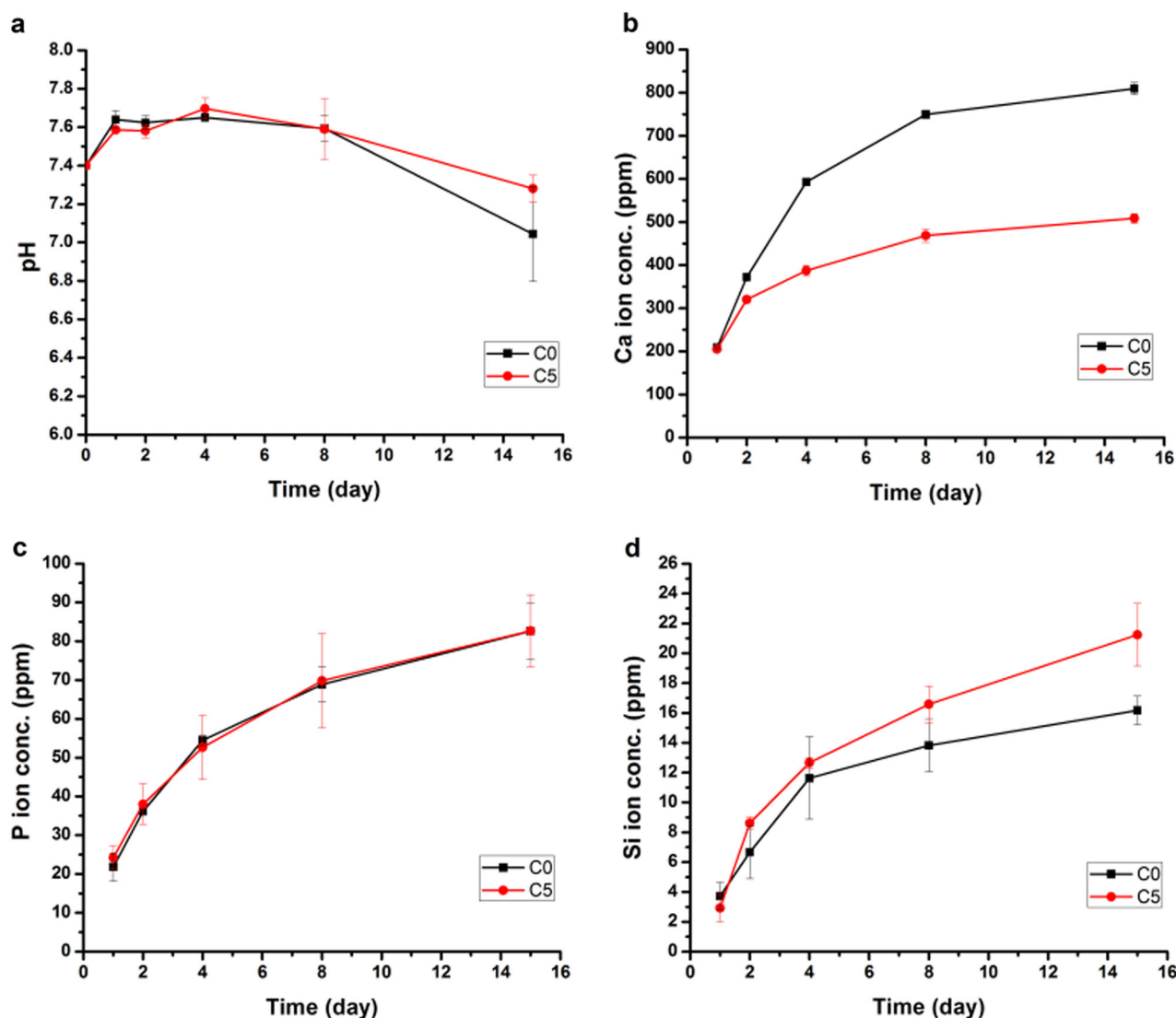


Fig. 6 pH a value of SBF solution and cumulative concentrations of Ca, P, and Si ions (b–d, respectively) released from samples C0 and C5 into SBF solution up to 15 days

of hydroxyl groups in the solution, and so, rising of fluid pH. This exchange resulted in breaking of Si–O–Si glass network bonds and formed silica-rich layer composed mainly of SiOH (silanol) groups on the glass surfaces. This newly formed layer possessed the affinity to attract Ca^{2+} and PO_4^{3-} from the surrounding solution and subsequently formed bone-like apatite crystals [50]. pH values were almost constant between 2 and 8 days, while, they decreased to 7.04 and 7.28 for C0 and C5, respectively, at the end of incubation period. This decrease attributed to the formation of the apatite layer on the glass surface.

The change of concentrations of Ce, Ca, P, and Si ions in SBF were also investigated as a sign of hydroxyapatite formation on the glass surfaces. Figure 6b–d shows the cumulative concentration of Ca, P, and Si ions in SBF solution incubated C0 and C5 glasses. Moreover, the

cumulative concentrations were fitted with the square root of time (the figure is not shown) to calculate the ions release rates. The concentration of Ce ions released into the solution was too low to be measured (<1 ppm). It can be noted from the figure that all ions were released in a two-stage profile. The first stage was a rapid release stage which was observed between 1 and 4 days. The second stage was a slow release stage which occurred from 4 days to the end of the immersion time. A fast first stage release rate can be assigned to the dissolution of different ions from the glass surfaces into SBF, while, a slow second stage release due to the precipitation of the calcium phosphate layer on their surfaces [50]. The concentration of Ca^{2+} ions in SBF incubated C0 was higher than that incubated C5 glass. That was because of a more depletion of Ca^{2+} ions in formation of calcium phosphate crystals in case of the fluid incubated

Table 2 The release rates (ppm.d^{-0.5}) of P, Ca, and Si ions from the samples C0 and C5 into SBF

	Ca		P		Si	
	1 st stage	2 nd stage	1 st stage	2 nd stage	1 st stage	2 nd stage
C0	383.8	113.1	32.6	15.0	8.0	2.4
C5	177.8	63.7	28.2	15.9	9.5	4.6

C5 glass. However, the difference in the cumulative Ca²⁺ ions concentrations was insignificant ($p > 0.05$) at 1 day, but they became significant at 2 and 4 days during the first release stage, where, the computed rates were 383.8 and 177.8 ppm.d^{-0.5} for C0 and C5, respectively (Table 2), whereas, the difference became significant ($p < 0.05$) in all times during the second stage (the release rates were 113.1 and 63.7 ppm.d^{-0.5} for C0 and C5, respectively). The release profiles of P ions from C0 and C5 glasses were almost typical. The first stage release rates were 32.6 and 28.2 ppm.d^{-0.5} and they were in the second stage 15.0 and 15.9 ppm.d^{-0.5} for C0 and C5, respectively. The concentration of Si⁴⁺ ions in SBF incubated C5 was higher than that incubated C0 glass which indicated a higher bioactivity of C5 glass surface than C0 one. The higher reactivity can be ascribed to higher number of NBOs generated the glass network by Ce addition. The calculated release rates of Si⁴⁺ ions in the first stage were found to be 8.0 and 9.5 ppm.d^{-0.5} and in the second stage they calculated as 2.4 and 4.6 ppm.d^{-0.5} for C0 and C5, respectively

3.6 Cytocompatibility evaluation

Figure 7 shows the results of viability tests of human lung fibroblast normal cell line (WI-38 cells) incubated with as prepared glass powders as a function of powder concentrations 0, 7.8, 15.6, 31.25, 62.5, 125, 250, 500, and 1000 µg/ml. The percentage of viability was determined by the ratio between the number of surviving cells in the medium exposed to the powder sample concentration and the number of surviving cells in a control medium. The results demonstrated that both glasses improved the growth conditions for cells which might reduce the stress on the cells. At low concentrations (0–31.25 µg/ml), the viability differences were in significant between C0 and C5 glasses, while, the differences became significant ($p < 0.05$) at high concentrations (62.5–1000 µg/ml). Where, C5 glass showed a significant higher viability than C0 glass. This can be elucidated by the degradation results. Aforementioned results showed that Si⁴⁺ ions concentration released into SBF from C5 was higher than that released from C0. Si⁴⁺ ions are known to adhere rapidly to fibroblast membranes [51], and consequently, C5 glass has improved the cell viability more than C0 glass. However, a high glass powder

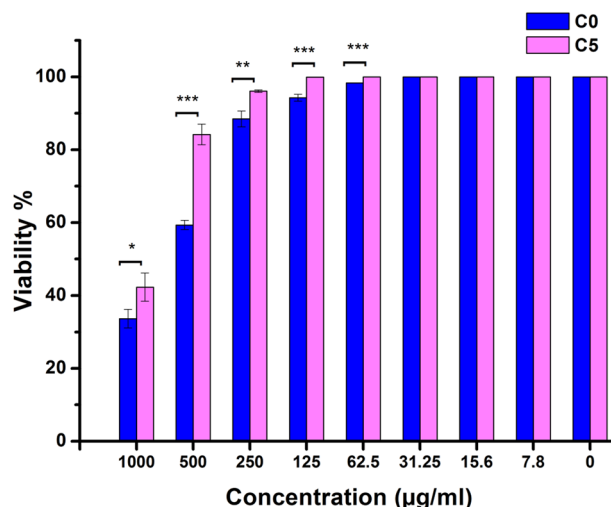


Fig. 7 Viability of normal human lung fibroblast cells (WI-38 cells) exposed to different concentrations (0, 7.8, 15.6, 31.25, 62.5, 125, 250, 500, and 1000 µg/ml) of C0 and C5 glasses powders after 24 h incubation. The cytotoxicity was determined by MTT assay. P -value obtained by Student's t -test (* $P < 0.05$, ** $P < 0.005$, and *** $P < 0.0001$)

concentrations were decreased significantly the viability as a result of a high ions release from the glasses. CC₅₀ for C5 glass was 909 µg/ml, while for C0 it was 682 µg/ml. Thus, addition of Ce to the glass increased the viability of cells.

Figure 8 shows inverted microscope images of human lung fibroblast normal cell line (WI-38 cells) with and without bioactive glass samples (C0 and C5) after incubation of the cells for 24 h at 37 °C. At concentration 250 µg/ml, both samples shows minimum cytotoxic effect, while at higher concentrations (500 and 1000 µg/ml) morphological changes were observed. In C5 sample morphological changes were smaller than that for C0.

3.7 Antibacterial activity

Antibacterial activity of C0 and C5 glass powders against gram negative bacteria (*Escherichia coli* and *Pseudomonas aeruginosa*) and gram positive bacteria (*Bacillus subtilis* and *Staphylococcus aureus*) was examined by measuring their inhibition zones diameters (IZD) (mm). Table 3 presents the inhibition zone diameter (mm) of both glasses against different bacteria used in this study. In general, both glass samples showed antibacterial activity against all studied bacteria. C0 sample demonstrated a weak effect on *Bacillus subtilis* (14.0 mm), while, its effect on *Staphylococcus aureus* was slightly increased to 16.0 mm. The highest effect of C0 glass was found for gram negative bacteria (*Pseudomonas aeruginosa* and *Escherichia coli*) with 19.0 and 20.0 mm, respectively. In contrast, C5 glass showed a weak effect on *Staphylococcus aureus* (14.0 mm), while it gave a moderate effect on *Bacillus subtilis* and

Fig. 8 Inverted microscope images of human lung fibroblast normal cell line (WI-38 cells) with and without glass nanoparticles (C0 and C5) after incubation of the cells for 24 h at 37 °C. **a** control WI-38 cells without glass particles. **b–d** are WI-38 cells with glass C0 concentration of 250, 500, and 1000 µg/ml, respectively. **e–g** are WI-38 cells with glass C5 concentration of 250, 500, and 1000 µg/ml, respectively). Magnification: ×40

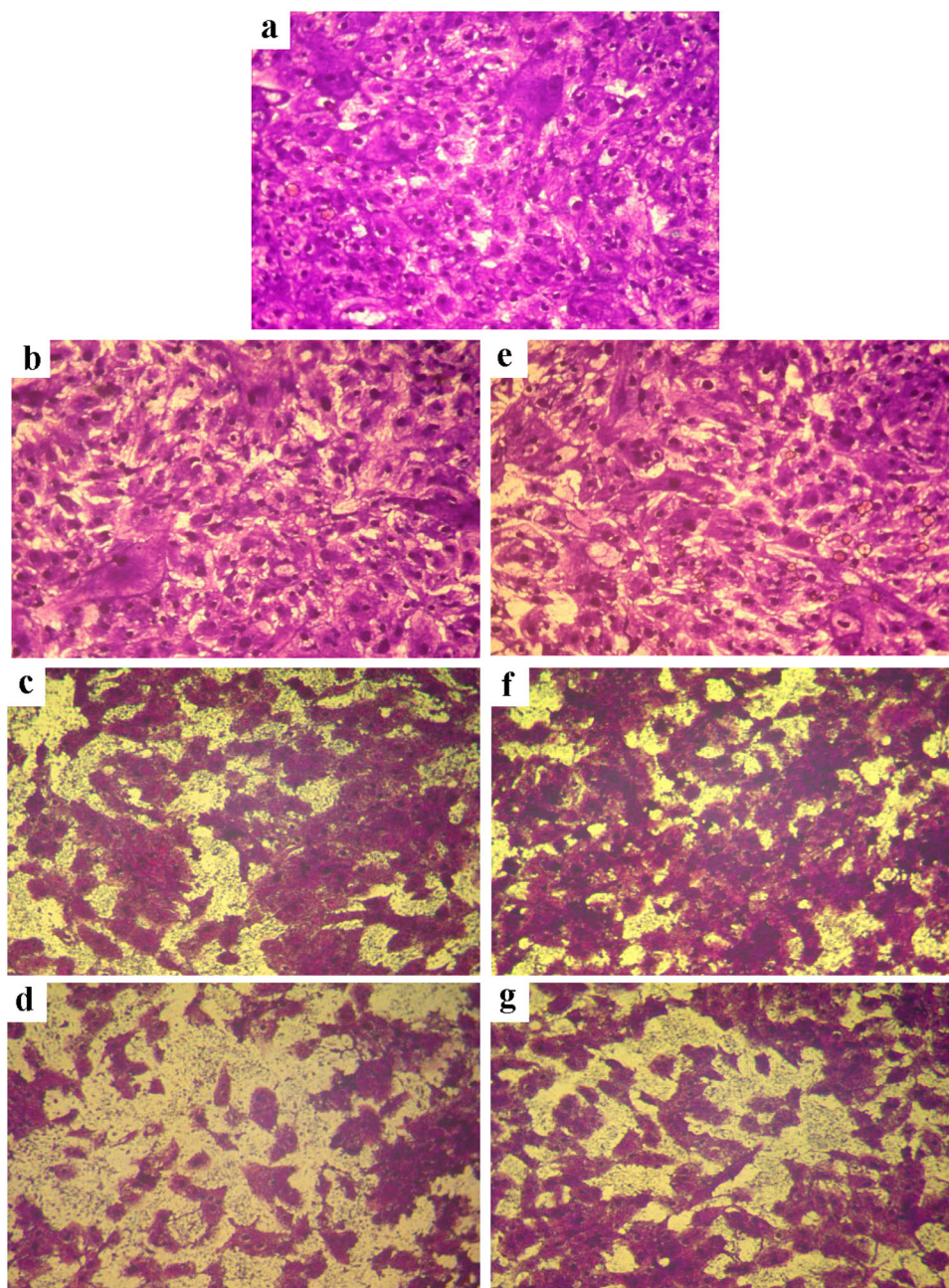


Table 3 Inhibitory activity of C0 and C5 against different types of bacteria (zone of inhibition in mm)

Type of bacteria		Inhibition zone diameter (mm)	
		C0	C5
Gram Negative Bacteria	<i>Escherichia coli</i>	20.0	21.0
	<i>Pseudomonas aeruginosa</i>	19.0	17.0
Gram Positive Bacteria	<i>Bacillus subtilis</i>	14.0	17.0
	<i>Staphylococcus aureus</i>	16.0	14.0

Pseudomonas aeruginosa providing equal inhibition zone diameter (17.0 mm), whereas, it donated the highest effect on *Escherichia coli* (21.0 mm). These results deduced that the antibacterial activity did not depend on a modification of the glass by cerium addition. It was likely due to a presence of boron in both glasses. Boron demonstrated notable antibacterial activity against a wide range of pathogens (bacteria, yeast, and fungi) [18, 19]. Interestingly, beside a development of bioactivity and cell stimulation by addition of cerium to the glass, addition of boron to the both glasses displayed showed a remarkable antibacterial activity against different kinds of bacteria.

3.8 Drug delivery

Figure 9b shows the percentage of ciprofloxacin loaded on C0 and C5 samples. From the figure it can be noted that sample C5 was loaded with significantly higher drug percentage (81.5 %) than that of sample C0 (76.7 %). As a consequence, the addition of Ce on the glass increased ciprofloxacin uptake. This can be explained by the ability of ciprofloxacin molecules (Fig. 9a) to coordinate through pyridone oxygen and one carboxylate oxygen to the metal [52]. Moreover, the drug molecules likely bond to the glass surface via hydrogen bonding formation between silica-rich layer (SiOH groups) and ciprofloxacin function groups (–OH, N–H, and –C=O).

Different parameters were studied for ciprofloxacin release (as a drug model) from glass nanoparticles. They included the type of carriers by modification of glass with Ce and the type of immersing media by incorporation phosphate ions and/or superoxide species (H₂O₂) to investigate the efficacy of this drug delivery system in different environment. Figure 9c, d represents the drug release in phosphate-free (tris-HCl buffer) and phosphate-contained (PBS) solutions with/without H₂O₂ as an oxidative reagent. Additional abbreviations were added to glass codes to indicate the type of solution in which the sample was immersed (H = H₂O₂). In general for all samples, the drug release profiles occurred by a sustained manner in two stages; the fast release stage which arose during the initial 12 h of soaking, it caused by the release of physically attached drug molecules at the glass surface. This stage followed by the slow release stage up to the end of incubation (168 h); it produced by the release of penetrated drug molecules inside glass pores. The percentages of drug released after 12 h of incubation were 32, 25, 35, 36, 33, 30, 36, and 36% (Table 4), while that released at the end of immersion time were 69, 52, 80, 83, 76, 72, 85, and 80% for C0-Tris, C5-Tris, C0-Tris-H, C5-Tris-H, C0-PBS, C5-PBS, C0-PBS-H, and C5-PBS-H, respectively. Additionally, the range of drug release amounts after 12 h of immersion was 0.19–0.30 mg/ml. Which is higher than the minimum inhibition concentration of ciprofloxacin for different pathogens [53]. The following paragraphs represented the effect of each parameter on the drug release profile.

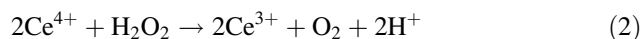
3.8.1 Effect of Ce addition to the glass

The plotted graphs revealed that the drug release was obviously affected by modification of glass with Ce addition. Ce-modified glass (C5 sample) showed lower drug release percentage when compared to Ce-free glass (C0 sample) in the same soaking medium. But, the differences decreased for PBS with and without H₂O₂. As previously mentioned, ciprofloxacin has high affinity to form

complexes with several metals and rare earth metals by forming ligand to the metal through the pyridone oxygen and one carboxylate oxygen [52]. Therefore, ciprofloxacin can be more attracted to the glass surface via coordination with Ce ions, and so, its detachment from glass surfaces became hard compared to Ce-free glass. On the other hand, there was a possibility to form hydrogen bonding between silanol (SiOH) groups formed on the glass surface in the aqueous medium and ciprofloxacin function groups (–OH, N–H, and –C=O). The silanol groups excite at silicate glass-water interface by hydrolysis of Si–O by either H⁺ or H₃O⁺ ions, specifically, non-birding oxygens (NBOs) have kinetically greater ability to be hydrolyzed and form SiOH groups. As mentioned before in FTIR spectra, addition of Ce (C5 sample) increased the number of NBOs in the glass network, and consequently, the number of formed silanol groups was higher in aqueous medium for C5 than C0 glass. In this case, the drug can be formed more hydrogen bonding and more stacked to C5 surface than C0. Accordingly, drug loading and release can be tailored and controlled by adjustment of glass with cerium.

3.8.2 Effect of H₂O₂ addition to the soaking media

Presence of H₂O₂ in the immersion fluids increased the percentage of drug release, but did not alter the drug release profile (Fig. 9c, d). This effect was more influential in the phosphate-free fluid (tris-HCl buffer) than that included phosphate ions (PBS). It was observed that the color of Ce-modified glass powders (C5 sample) was changed from pale yellow to deep yellow-orange color when immersed in solutions included H₂O₂ after few hours of immersion, and this color continued throughout the whole soaking time. This color change was likely attributed to the oxidation of Ce³⁺ (pale yellow) on the glass surface to Ce⁴⁺ (yellow–orange) [54]. This was an indication for the oxidizing action of H₂O₂ and the catalytic ability of Ce on the glass surface to decompose H₂O₂. This reaction mechanism can be showed as follows: [55]



Therefore, H₂O₂ can be decomposed by Ce³⁺ to H₂O according to Eq. 1 and form Ce⁴⁺ ions on the glass surface which in turn destroyed H₂O₂ to O₂ and H⁺ according to Eq. 2. These two reactions can be summated to give reaction in Eq. 3. This catalytic cycle of Ce was almost decrease or discarded the ligand capacity of ciprofloxacin molecule to Ce ions on the glass surface. Moreover, according to Eqs.

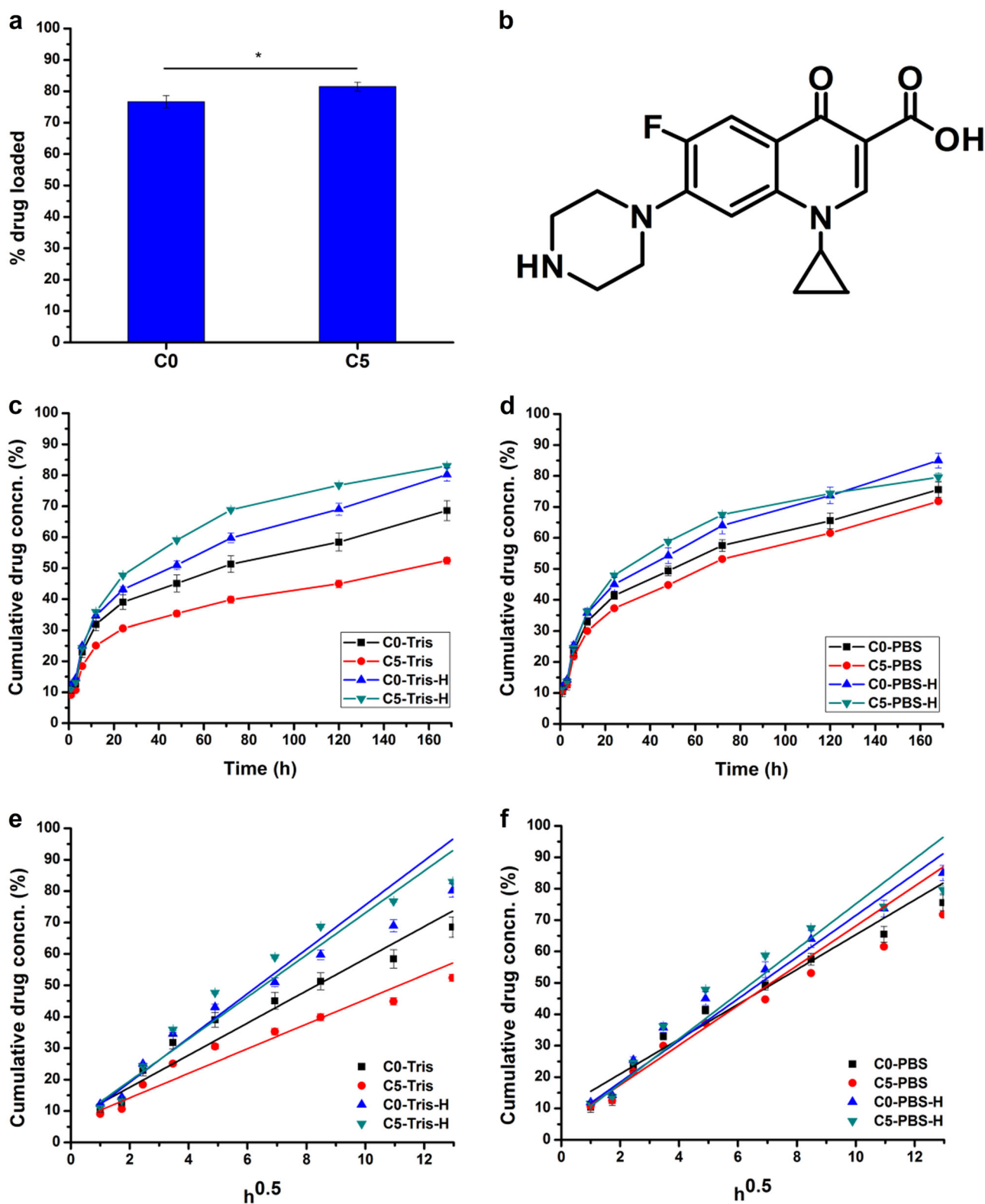


Fig. 9 Percentage of loaded drug **a**, Ciprofloxacin chemical structure **b**, cumulative percentage of drug release in tris-HCl buffer and PBS with/without H_2O_2 (**c**, **d**, respectively) and corresponding data linear fitting with Higuchi model (**e**, **f**, respectively) of C0 and C5 glass

nanoparticles. Additional abbreviations were added to glass codes to indicate the type of solution in which the sample was immersed (H = H_2O_2)

Table 4 The cumulative % of released drug from C0 and C5 samples into Tris, Tris-H₂O₂, PBS, and PBS-H₂O₂ after 12 h and 168 h of immersion

	C0-Tris	C5-Tris	C0-Tris-H	C5-Tris-H	C0-PBS	C5-PBS	C0-PBS-H	C5-PBS-H
12 h	32	25	35	36	33	30	36	36
168 h	69	52	80	83	76	72	85	80

Table 5 Higuchi constant, k (h^{-0.5}), and regression coefficient (R^2) calculated from Higuchi model

	C0-Tris	C5-Tris	C0-Tris-H	C5-Tris-H	C0-PBS	C5-PBS	C0-PBS-H	C5-PBS-H
k (h ^{-0.5})	5.12	3.92	7.05	6.69	5.54	6.33	6.64	7.16
R^2	0.942	0.927	0.905	0.955	0.939	0.908	0.957	0.881

1, 2, and 3, Ce presented on the glass surface was disintegrated 2 moles of H₂O₂ to give 2 moles of water and 1 mole of oxygen molecules. By this way, the concentration of water molecules was increased at the glass surface and sequentially increased glass dissolution. On the other hand, these water molecules likely weakened the hydrogen bond developed between glass surface and drug molecules. Where, hydrogen bonds can be formed between drug molecules and these water molecules instead of forming such bonds between the glass surface and drug molecules. All of these circumstances can facilitated drug release from the solutions including H₂O₂, and this explained a higher drug release in these solutions.

3.8.3 Effect of phosphate ions in the soaking media

Likewise, the drug release profiles of different samples did not altered as a result of presence of phosphate ions in the soaking solutions. However, the percentage differences of released drug were reduced regardless the consistence of H₂O₂ in the solution (Fig. 9d). This can be explained by the affinity of ciprofloxacin molecule to form an ionic bond between the negatively charged phosphate ion presented in the solution and the positively charged piperazine ring in ciprofloxacin molecule. This hypothesis was derived from previous works which showed the interaction rout of ciprofloxacin with phosphate group in phospholipids [56–58]. From another side of view, Ce atoms have a tendency to bond with phosphate species and forms insoluble CePO₄ crystals which increased the glass surface durability [12]. At the same time, they inhibited the contact of H₂O₂ with Ce on the glass surface, and so, preventing its decomposition efficacy by Ce-modified glass surface. Furthermore, formation of such crystals decreased the coordination capability of ciprofloxacin with Ce ions. These conditions caused a relatively high release in phosphate buffer solution.

3.8.4 Drug releasing kinetics

The mechanism of drug release was investigated by linear fitting of the data with Higuchi model [40] (Fig. 9e, f).

The degree of linearity was determined from regression coefficient (R^2), Higuchi constant, k (h^{-0.5}) calculated as well and represented in Table 5. For all samples, R^2 values were found to be >0.9 (except for C5-PBS-H, it was <0.9) which indicated that the release mechanism was controlled by Fickian diffusion. The highest R^2 values were calculated for C0-PBS-H (0.957), while the lowest one was found for C5-PBS-H (0.881), and consequently, the solution kind influenced the release mechanism of the drug. Moreover, the drug release rate was affected dominantly by glass type specifically in the solution free from hydrogen peroxide and phosphate ions. C5 showed the lowest drug release rate (3.92 h^{-0.5}) in tris-HCl buffer (C5-Tris sample), but it showed the highest release rate and nearly twice multiplied (7.16 h^{-0.5}) when it immersed in PBS contained hydrogen peroxide (C5-PBS-H sample). Accordingly, the drug release kinetics was influenced by the composition of glass carriers and the environment of soaking medium.

4 Conclusion

In the present study a new novel nano-bioactive glass contained B and Ce was prepared successfully. The influence of Ce-doping on bioactivity, cytocompatibility, antibacterial activity, and ciprofloxacin delivery were investigated. Furthermore, the effect of soaking medium nature on ciprofloxacin release behavior was examined. Where, phosphate-free (tris-HCl buffer) and phosphate-containing (PBS) solutions with/without H₂O₂ were used to mimic the drug release in ROS environment. Ce addition improved hydroxyapatite formation and cell viability. In addition, Ce-free and Ce-doped glasses were showed antibacterial activity against different kinds of bacteria. This was assigned to the presence of boron in both glasses. Ciprofloxacin release behavior was affected by a presence of H₂O₂, especially for Ce-doped glass, while the phosphate species showed a slight influence. We concluded from this study that effect of oxidative stress on the drug release behavior have to be taken into consideration, specifically when antioxidant materials used as drug carriers.

Acknowledgements We would like to thank the National Research Center, Faculty of Science and Al-Azhar University (Girls), Egypt for a possibility to use their facilities.

Compliance with ethical standards

Conflict of interest The authors declare that they have no conflict of interest.

Publisher's note Springer Nature remains neutral with regard to jurisdictional claims in published maps and institutional affiliations.

References

- Chen J, Patil S, Seal S, McGinnis JF. Rare earth nanoparticles prevent retinal degeneration induced by intracellular peroxides. *Nat Nanotechnol.* 2006;1:142–50.
- Korsvik C, Patil S, Seal S, Self WT. Superoxide dismutase mimetic properties exhibited by vacancy engineered ceria nanoparticles. *Chem Commun.* 2007;1056–8. <https://doi.org/10.1039/B615134E>.
- Pirmohamed T, Dowding JM, Singh S, Wasserman B, Heckert E, Karakoti AS, et al. Nanoceria exhibit redox state-dependent catalase mimetic activity. *Chem Commun.* 2010;46:2736–8.
- Du J, Kokou L, Rygel JL, Chen Y, Pantano CG, Woodman R, et al. Structure of cerium phosphate glasses: molecular dynamics simulation. *J Am Ceram Soc.* 2011;94:2393–401.
- Leonelli C, Lusvardi G, Malavasi G, Menabue L, Tonelli M. Synthesis and characterization of cerium-doped glasses and in vitro evaluation of bioactivity. *J Non-Cryst Solids.* 2003;316:198–216.
- Goh Y-F, Alshemary AZ, Akram M, Kadir MRA, Hussain R. In-vitro characterization of antibacterial bioactive glass containing ceria. *Ceram Int.* 2014;40:729–37.
- Shruti S, Salinas AJ, Malavasi G, Lusvardi G, Menabue L, Ferrara C, et al. Structural and in vitro study of cerium, gallium and zinc containing sol–gel bioactive glasses. *J Mater Chem.* 2012;22:13698–706.
- Zhang J, Liu C, Li Y, Sun J, Wang P, Di K, et al. Effect of cerium ion on the proliferation, differentiation and mineralization function of primary mouse osteoblasts in vitro. *J Rare Earths.* 2010;28:138–42.
- Deliormanlı AM. Synthesis and characterization of cerium- and gallium-containing borate bioactive glass scaffolds for bone tissue engineering. *J Mater Sci Mater Med.* 2015;26:67.
- Gupta B, Papke JB, Mohammadkhah A, Day DE, Harkins AB. Effects of chemically doped bioactive borate glass on neuron regrowth and regeneration. *Ann Biomed Eng.* 2016;44:3468–77.
- Nicolini V, Malavasi G, Menabue L, Lusvardi G, Benedetti F, Valeri S, et al. Cerium-doped bioactive 45S5 glasses: spectroscopic, redox, bioactivity and biocatalytic properties. *J Mater Sci.* 2017;52:8845–57.
- Nicolini V, Varini E, Malavasi G, Menabue L, Menziani MC, Lusvardi G, et al. The effect of composition on structural, thermal, redox and bioactive properties of Ce-containing glasses. *Mater Des.* 2016;97:73–85.
- Placek L, Keenan T, Coughlan A, Wren A. Investigating the effect of glass ion release on the cytocompatibility, antibacterial efficacy and antioxidant activity of Y_2O_3/CeO_2 doped $SiO_2-SrO-Na_2O$ glasses. *Biomed Glass.* 2018;4:32–44.
- Nicolini V, Gambuzzi E, Malavasi G, Menabue L, Menziani MC, Lusvardi G, et al. Evidence of catalase mimetic activity in Ce^{3+}/Ce^{4+} doped bioactive glasses. *J Phys Chem B.* 2015;119:4009–19.
- Devirian TA, Volpe SL. The physiological effects of dietary boron. *Crit Rev Food Sci Nutr.* 2003;43:219–231.
- Chapin RE, Ku WW, Kenney MA, McCoy H. The effects of dietary boric acid on bone strength in rats. *Biol Trace Elem Res.* 1998;66:395–9.
- Uysal T, Ustdal A, Sonmez MF, Ozturk F. Stimulation of bone formation by dietary boron in an orthopedically expanded suture in rabbits. *Angle Orthod.* 2009;79:984–90.
- De Seta F, Schmidt M, Vu B, Essmann M, Larsen B. Antifungal mechanisms supporting boric acid therapy of *Candida* vaginitis. *J Antimicrob Chemother.* 2008;63:325–36.
- Qin G, Zong Y, Chen Q, Hua D, Tian S. Inhibitory effect of boron against *Botrytis cinerea* on table grapes and its possible mechanisms of action. *Int J Food Microbiol.* 2010;138:145–50.
- Wu C, Miron R, Sculean A, Kaskel S, Doert T, Schulze R, et al. Proliferation, differentiation and gene expression of osteoblasts in boron-containing associated with dexamethasone deliver from mesoporous bioactive glass scaffolds. *Biomaterials.* 2011;32:7068–78.
- Durand LAH, Vargas GE, Romero NM, Vera-Mesones R, Porto-López JM, Boccaccini AR, et al. Angiogenic effects of ionic dissolution products released from a boron-doped 45S5 bioactive glass. *J Mater Chem B.* 2015;3:1142–8.
- Seyedmomeni SS, Naeimi M, Raz M, Mohandesi JA, Moztarzadeh F, Baghbani F, et al. Synthesis, characterization and biological evaluation of a new sol-gel derived B and Zn-containing bioactive glass: in vitro study. *Silicon.* 2018;10:197–203.
- Balasubramanian P, Hupa L, Jokic B, Detsch R, Grünwald A, Boccaccini AR. Angiogenic potential of boron-containing bioactive glasses: in vitro study. *J Mater Sci.* 2017;52:8785–92.
- El-Kady AM, Farag MM, El-Rashedi AM. Bioactive glass nanoparticles designed for multiple deliveries of lithium ions and drugs: curative and restorative bone treatment. *Eur J Pharm Sci.* 2016;91:243–50.
- Shruti S, Salinas AJ, Ferrari E, Malavasi G, Lusvardi G, Doadrio AL, et al. Curcumin release from cerium, gallium and zinc containing mesoporous bioactive glasses. *Microporous Mesoporous Mater.* 2013;180:92–101.
- Zhang Y, Wang X, Su Y, Chen D, Zhong W. A doxorubicin delivery system: samarium/mesoporous bioactive glass/alginate composite microspheres. *Mater Sci. Eng C Mater Biol. Appl.* 2016;67:205–13.
- Lee J-H, Mandakhbayar N, El-Fiqi A, Kim H-W. Intracellular co-delivery of Sr ion and phenamil drug through mesoporous bio-glass nanocarriers synergizes BMP signaling and tissue mineralization. *Acta Biomater.* 2017;60:93–108.
- Xue Y, Du Y, Yan J, Liu Z, Ma PX, Chen X, et al. Monodisperse photoluminescent and highly biocompatible bioactive glass nanoparticles for controlled drug delivery and cell imaging. *J Mater Chem B.* 2015;3:3831–9.
- Singh R, Singh S. Role of phosphate on stability and catalase mimetic activity of cerium oxide nanoparticles. *Colloids Surf B Biointerfaces.* 2015;132:78–84.
- Singh S, Dosani T, Karakoti AS, Kumar A, Seal S, Self WT. A phosphate-dependent shift in redox state of cerium oxide nanoparticles and its effects on catalytic properties. *Biomaterials.* 2011;32:6745–53.
- Xia W, Chang J. Preparation and characterization of nano-bioactive-glasses (NBG) by a quick alkali-mediated sol–gel method. *Mater Lett.* 2007;61:3251–3.
- Kokubo T, Takadama H. How useful is SBF in predicting in vivo bone bioactivity? *Biomaterials.* 2006;27:2907–15.
- Mosmann T. Rapid colorimetric assay for cellular growth and survival: application to proliferation and cytotoxicity assays. *J Immunol Methods.* 1983;65:55–63.

34. MacFaddin J. Media for isolation-cultivation-identification-maintenance of medical bacteria. Vol. 1, Williams and Wilkins: Baltimore; 1985.
35. Lapage S, Shelton J, Mitchell T. Methods in microbiology. Academic Press, London, 1970;3A.
36. Clesceri L, Greenberg A, Eaton A. Standard methods for the examination of water and wastewater, American Public Health Association (APHA), American Water Works Association, Water Environment Federation, Washington, DC. Standard methods for the examination of water and wastewater, 20th ed American Public Health Association (APHA), American Water Works Association, Water Environment Federation, Washington, DC. 1998.
37. Barry A. Procedure for testing antimicrobial agents in agar media: theoretical considerations. *Antibiot Lab Med.* 1986;2:1–26.
38. Rahman MU, Gul S, Haq MZU. Reduction of chromium (VI) by locally isolated *Pseudomonas* sp. C-171. *Turk J Biol.* 2007;31:161–6.
39. Motwani SK, Chopra S, Talegaonkar S, Kohli K, Ahmad FJ, Khar RK. Chitosan–sodium alginate nanoparticles as submicroscopic reservoirs for ocular delivery: formulation, optimisation and in vitro characterisation. *Eur J Pharm Biopharm.* 2008;68:513–25.
40. Higuchi T. Mechanism of sustained-action medication. Theoretical analysis of rate of release of solid drugs dispersed in solid matrices. *J Pharm Sci.* 1963;52:1145–9.
41. Ashuri M, Moztarzadeh F, Nezafati N, Hamedani AA, Tahriri M. Development of a composite based on hydroxyapatite and magnesium and zinc-containing sol–gel-derived bioactive glass for bone substitute applications. *Mater Sci Eng C.* 2012;32:2330–9.
42. Saboori A, Rabiee M, Moztarzadeh F, Sheikhi M, Tahriri M, Karimi M. Synthesis, characterization and in vitro bioactivity of sol-gel-derived SiO₂–CaO–P₂O₅–MgO bioglass. *Mater Sci Eng C.* 2009;29:335–40.
43. Goh Y-F, Alshemary AZ, Akram M, Kadir MRA, Hussain R. In vitro study of nano-sized zinc doped bioactive glass. *Mater Chem Phys.* 2013;137:1031–8.
44. Montazerian M, Schneider JF, Yekta BE, Marghussian VK, Rodrigues AM, Zanotto ED. Sol–gel synthesis, structure, sintering and properties of bioactive and inert nano-apatite–zirconia glass-ceramics. *Ceram Int.* 2015;41:11024–45.
45. Aguiar H, Solla E, Serra J, González P, León B, Almeida N, et al. Orthophosphate nanostructures in SiO₂–P₂O₅–CaO–Na₂O–MgO bioactive glasses. *J Non-Cryst Solids.* 2008;354:4075–80.
46. Zhang E, Zou C, Yu G. Surface microstructure and cell biocompatibility of silicon-substituted hydroxyapatite coating on titanium substrate prepared by a biomimetic process. *Mater Sci Eng C.* 2009;29:298–305.
47. Deliormanlı AM, Yıldırım M. Sol-gel synthesis of 13-93 bioactive glass powders containing therapeutic agents. *J Aust Ceram Soc Vol.* 2016;52:9–19.
48. Oliveira J, Correia R, Fernandes M. Effects of Si speciation on the in vitro bioactivity of glasses. *Biomaterials.* 2002;23:371–9.
49. Hesaraki S, Gholami M, Vazehrad S, Shahrabi S. The effect of Sr concentration on bioactivity and biocompatibility of sol-gel derived glasses based on CaO–SrO–SiO₂–P₂O₅ quaternary system. *Mater Sci Eng C.* 2010;30:383–90.
50. Kokubo T, Ito S, Huang Z, Hayashi T, Sakka S, Kitsugi T, et al. Ca, P-rich layer formed on high-strength bioactive glass-ceramic A-W. *J Biomed Mater Res A.* 1990;24:331–43.
51. Absher M, Mortara M. Effect of silica on the proliferative behavior of human lung fibroblasts. *In Vitro Cell Dev Biol Plant.* 1980;16:371–6.
52. Uivarosi V. Metal complexes of quinolone antibiotics and their applications: an update. *Molecules.* 2013;18:11153–97.
53. Andrews JM. Determination of minimum inhibitory concentrations. *J Antimicrob Chemother.* 2001;48:5–16.
54. Xu C, Qu X. Cerium oxide nanoparticle: a remarkably versatile rare earth nanomaterial for biological applications. *NPG Asia. Materials.* 2014;6:e90.
55. Celardo I, Pedersen JZ, Traversa E, Ghibelli L. Pharmacological potential of cerium oxide nanoparticles. *Nanoscale.* 2011;3:1411–20.
56. Montero MT, Pijoan M, Merino-Montero S, Vinuesa T, Hernández-Borrell J. Interfacial membrane effects of fluoroquinolones as revealed by a combination of fluorescence binding experiments and atomic force microscopy observations. *Langmuir.* 2006;22:7574–8.
57. Grancelli A, Morros A, Cabañas ME, Domènech Ò, Merino S, Vázquez JL, et al. Interaction of 6-fluoroquinolones with dipalmitoylphosphatidylcholine monolayers and liposomes. *Langmuir.* 2002;18:9177–82.
58. Fresta M, Guccione S, Beccari AR, Furneri PM, Puglisi G. Combining molecular modeling with experimental methodologies: mechanism of membrane permeation and accumulation of ofloxacin. *Bioorg Med Chem.* 2002;10:3871–89.